

# High-Temperature Properties of Mold Flux Observed and Measured In Situ by Single/Double Hot-Thermocouple Technique

WANLIN WANG<sup>1</sup>,<sup>1</sup> PEISHENG LYU,<sup>1</sup> LEJUN ZHOU,<sup>1,2</sup> HUAN LI,<sup>1</sup>  
and TONGSHENG ZHANG<sup>1</sup>

1.—School of Metallurgy and Environment, Central South University, Changsha 410083, Hunan, China. 2.—e-mail: lj.zhou@hotmail.com

Mold flux plays very important roles in the continuous casting process, and its high-temperature properties affect the quality of the final as-cast product greatly. Investigations on the melting, isothermal and nonisothermal crystallization, and phase evolution behaviors under a simulated temperature field for the mold flux system using the single/double hot-thermocouple technique (S/DHTT) were reviewed. Meanwhile, further in situ observations on the wetting behavior and heat transfer ability of the mold flux system were also carried out using the S/DHTT. The results summarized here provide a clear understanding of both the high-temperature properties of mold flux and the detailed application of advanced real-time visual high-temperature S/DHTT to this molten slag system.

## INTRODUCTION

Continuous casting is one of the most important innovations in the steel industry due to its high yield, high product quality, energy savings, less pollution, lower cost, as well as better working conditions. In 2017, over 96% of crude steel was cast by continuous caster worldwide.<sup>1</sup> As an important slag, mold flux plays very important roles in the continuous casting process. It protects steel from oxidation, insulates it from freezing, and absorbs inclusions, when floating on top of liquid steel; whereas it lubricates the shell and moderates the heat transfer in the mold, when it infiltrates into the mold/shell channel. Therefore, the quality of the final cast product is greatly determined by the high-temperature properties of mold flux. Improper properties may lead to defects in the bloom, slab or billet, such as severe oscillation marks,<sup>2–5</sup> cracks,<sup>6–8</sup> inclusions and slag entrapment,<sup>9–12</sup> improper solidification structure distribution,<sup>13–15</sup> and even breakout.<sup>16,17</sup>

However, the actual situation in the mold cannot be observed directly due to its opacity, as well as the high in-mold temperature, transient fluid flow, complicated phase transitions and chemical reactions, etc.<sup>18,19</sup> To investigate the high-temperature

properties of mold flux, many kinds of methods and techniques have been utilized. The high-temperature microscopy technique<sup>20–22</sup> and single hot-thermocouple technique<sup>23–25</sup> are usually applied to investigate the melting behavior of mold flux. Differential thermal analysis (DTA),<sup>26–29</sup> the single/double hot-thermocouple technique (S/DHTT),<sup>30–34</sup> and confocal scanning laser microscopy (CSLM)<sup>35–37</sup> are often utilized to study its crystallization behavior. The infrared emitter technique (IET),<sup>25,38–41</sup> copper finger heat flux simulator,<sup>42,43</sup> Fourier-transform infrared (FTIR) spectrometry,<sup>44–47</sup> etc. are used to characterize the heat transfer performance of mold flux. Meanwhile, x-ray photography<sup>48,49</sup> and the sessile drop method<sup>50–52</sup> are good ways to observe its surface/interface behaviors. Moreover, high-temperature viscometry<sup>53–55</sup> is usually applied to study the rheological properties of mold flux.

The concept of SHTT was first presented by Ordway et al.<sup>56</sup> and Welch et al.<sup>57</sup> in the 1950s, with the potential to determine the melting point of slags, glass devitrification, growth of single crystals for x-ray structure determination, and delineation of phase equilibria. It has been widely used in the fields of slag, glass, and ceramic technology.<sup>58–62</sup> In 1997, the SHTT was first applied to investigate the

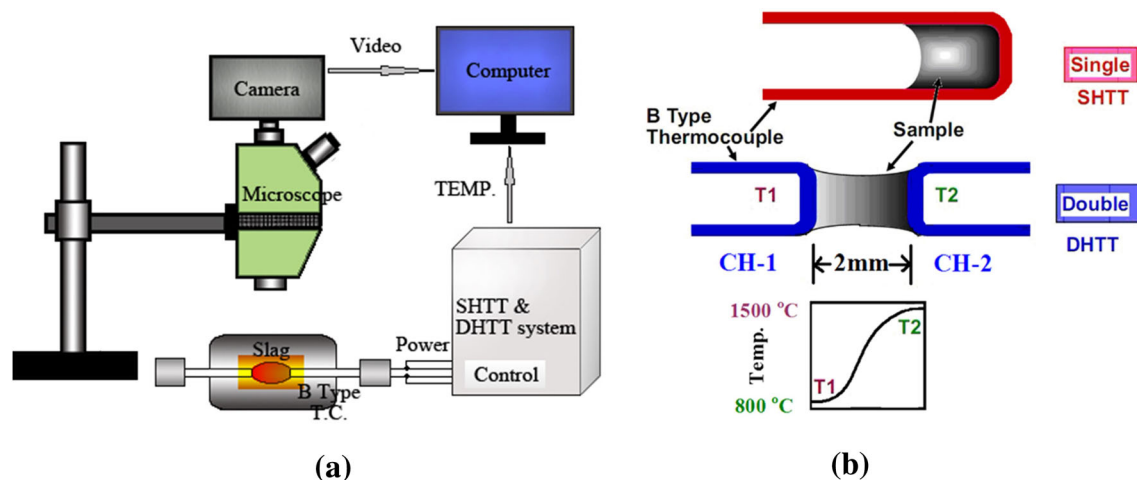


Fig. 1. Single/double hot-thermocouple technique: (a) schematic of apparatus and (b) SHTT and DHTT models.

crystallization behavior of a continuous casting mold flux by Kashiwaya et al.<sup>63</sup> Also, based on the SHTT, they further developed the DHTT by doubling the “U-shaped” B-type thermocouple and its associated controlling system.<sup>64</sup> Nowadays, both the SHTT and DHTT have become routine approaches for investigating the high-temperature properties of mold flux. Figure 1 shows a schematic of the S/DHTT apparatus. Details about the S/DHTT have been described in previous papers.<sup>64–66</sup>

### MELTING BEHAVIOR

The melting behavior of mold flux determines the thickness of the liquid slag layer at the top of the molten steel in the mold, which further affects the performance of the mold flux during the initial solidification of the molten steel.<sup>67–69</sup> The high-temperature microscopy technique has been used to obtain the temperature of the softening point, hemisphere point, and fluidity point of the mold flux, but its heating rate is greatly limited due to the output power of the heating furnace.<sup>20–22</sup> The heating rate also has a significant impact on the melting temperature range of mold flux, which usually increases at higher heating rate.<sup>70</sup> As the temperature of mold flux can reach 1273 K (1000°C) in a few seconds after being added to the continuous casting mold, high-temperature microscopy cannot properly reflect the real scenario of the melting behavior of the mold flux in the mold. However, the SHTT can achieve high heating and cooling rates due to its unique configuration, in which the heating rate can be varied from 0 K/s to 30 K/s.<sup>64,65</sup> Figure 2 shows the melting behavior of a mold flux as observed and measured by the SHTT.<sup>71</sup>

The principle of measuring the melting temperature range of mold flux using the SHTT is to utilize the temperature deviation between the curves for the preset heating rate and the temperature response data measured in real time during the

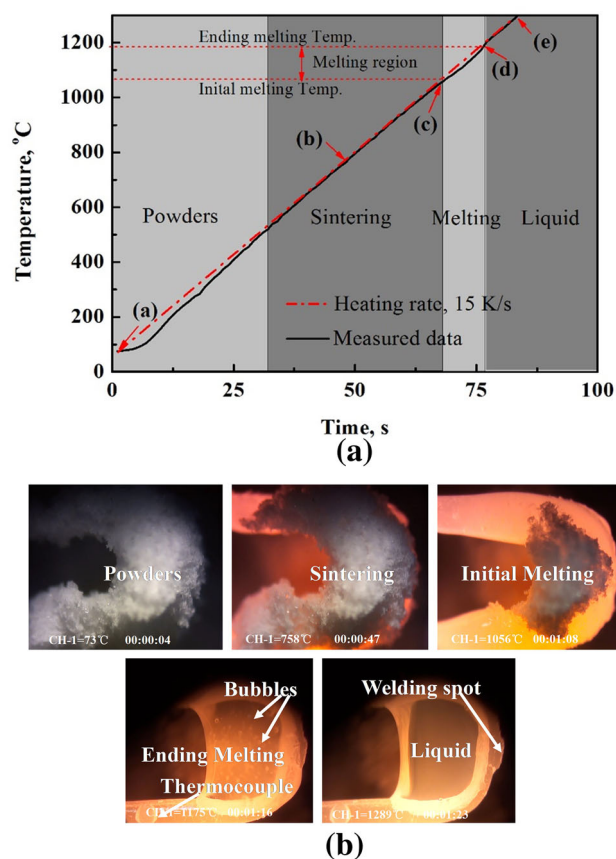


Fig. 2. Melting behavior of mold flux observed and measured using the SHTT.<sup>71</sup> (a) temperature history and (b) typical stages during melting process.

mold flux melting process, as shown in Fig. 2a. This deviation results from the endothermic reaction of the melting process. Besides, continuous in situ observation by charge-coupled device (CCD) camera of the mold flux variation from powders to sintering, initial melting, and final melting is also shown in

Fig. 2b, which enables the initial and complete melting temperature of the mold flux under the preset heat rate to be obtained accurately. The initial and complete melting temperatures for the sampled mold flux in Fig. 2 are 1329 K (1056°C) and 1448 K (1175°C), respectively.

### ISOTHERMAL CRYSTALLIZATION TRANSFORMATION

The crystallization ability of mold flux directly affects the dynamic phase transition and distribution of the mold flux film in the mold–shell gap, in turn influencing the heat transfer and lubrication performance of the mold flux. The reason is that the heat transfer capability and rheological properties of glassy, liquid, and crystalline mold flux are very different.<sup>72,73</sup> The isothermal crystallization transformation of mold flux can be studied by holding the sample at constant temperature for a certain time until the whole sample is fully crystallized. DTA is not suitable for such analysis of the isothermal crystallization transformation of mold flux due to its low heating/cooling rate, which cannot simulate the real scenario in the mold. However, both the S/DHTT and CSLM can achieve heating and cooling rates above 30 K/s, which can reduce errors introduced by precipitation of crystals during the heating or cooling process. Besides, exothermic peaks measured in DTA are used to characterize the crystallization process, whereas the S/DHTT and CSLM can observe crystal formation in situ from the molten or glassy mold flux through the development of opaque crystals. Figure 3a shows snapshots of the isothermal crystallization process of a mold flux at temperature of 1273 K (1000°C) using the SHTT. The crystalline fraction (nontransparent part,  $X$ ) in the sample increases with holding time.

Temperature–time transformation (TTT) diagrams of isothermal crystallization transformation can be constructed based on the crystalline fraction of mold flux at different times and holding temperatures obtained by SHTT measurements. Figure 3b shows such a TTT diagram for a mold flux with basicity of 1.2,<sup>65</sup> illustrating that the mold flux remains liquid when the temperature is higher than 1673 K (1400°C), whereas it is almost fully crystallized when the time is above the curve corresponding to 95% crystalline fraction. Between these, its state is a mixture of coexisting liquid and crystal. Also, it can be seen that the shape of the two curves is of “double C” type, indicating that different crystals precipitate in high- and low-temperature zones. The precipitated crystalline phase can be identified by x-ray diffraction (XRD) analysis, as shown in Fig. 3c, where calcium silicate ( $\text{CaO}\cdot\text{SiO}_2$ ) precipitated in the high-temperature zone but cuspidine ( $\text{Ca}_4\text{Si}_2\text{O}_7\text{F}_2$ ) in the low-temperature zone. Besides, based on the measured crystalline fraction versus time at different holding temperatures, kinetic studies of the isothermal crystallization

can be conducted using models such as that of Johnson–Mehl–Avrami (JMA), etc., and the mechanism of nucleation and growth of crystals in the mold flux can also be explored.<sup>65,74,75</sup>

### NONISOTHERMAL CRYSTALLIZATION TRANSFORMATION

The isothermal crystallization behavior can be used to characterize the crystallization ability of mold flux; however, mold flux in the casting mold also experiences nonisothermal process after infiltrating into the gap between the mold and the initial shell. Such nonisothermal crystallization transformation of mold flux can also be investigated using the SHTT by controlling the heating or cooling rate. Figure 4 shows an investigation of nonisothermal crystallization using the SHTT. Figure 4a shows snapshots of typical stages during the continuous cooling process,<sup>65,76</sup> where crystals precipitate continuously as the slag sample is cooled. Figure 4b shows the continuous cooling transformation (CCT) diagram of the mold flux with basicity of 1.2, which can be constructed by measuring the variation of the crystalline fraction with time for different cooling rates.

Two important parameters reflecting the crystallization behavior of the mold flux in the continuous cooling crystallization process can be obtained from such a CCT diagram, viz. the initial crystallization temperature ( $T_{IC}$ ) and the critical cooling rate ( $C_{CR}$ ). When the temperature is higher than the initial crystallization temperature, the mold flux remains liquid. Meanwhile, if the actual cooling rate is higher than the critical value, the molten mold flux will transform into glassy phase. The initial crystallization temperature of the mold flux at different cooling rates is shown in Fig. 4c. Generally, the initial crystallization temperature of mold flux decreases with increase of the cooling rate. This effect is due to the increase of the viscosity of the molten slag on increase of the cooling rate, requiring a greater driving force to initiate crystallization; In other words, greater undercooling is needed. Furthermore, the kinetics of nonisothermal crystallization transformation can also be analyzed based on the relationship between crystalline fraction, time, and cooling rate, using the developed nonisothermal kinetic models.<sup>76–79</sup> Moreover, the mechanism of nucleation and growth of crystals during such nonisothermal processes can be obtained based on the nonisothermal models mentioned above, providing fundamental guidance for controlling the size and morphology of precipitated crystals by adjusting kinetic factors.

### PHASE EVOLUTION UNDER A SIMULATED TEMPERATURE FIELD

In a continuous casting mold, a huge temperature gradient exists in the 2-mm-wide gap between the hot solidified shell and water-cooled mold wall. Most

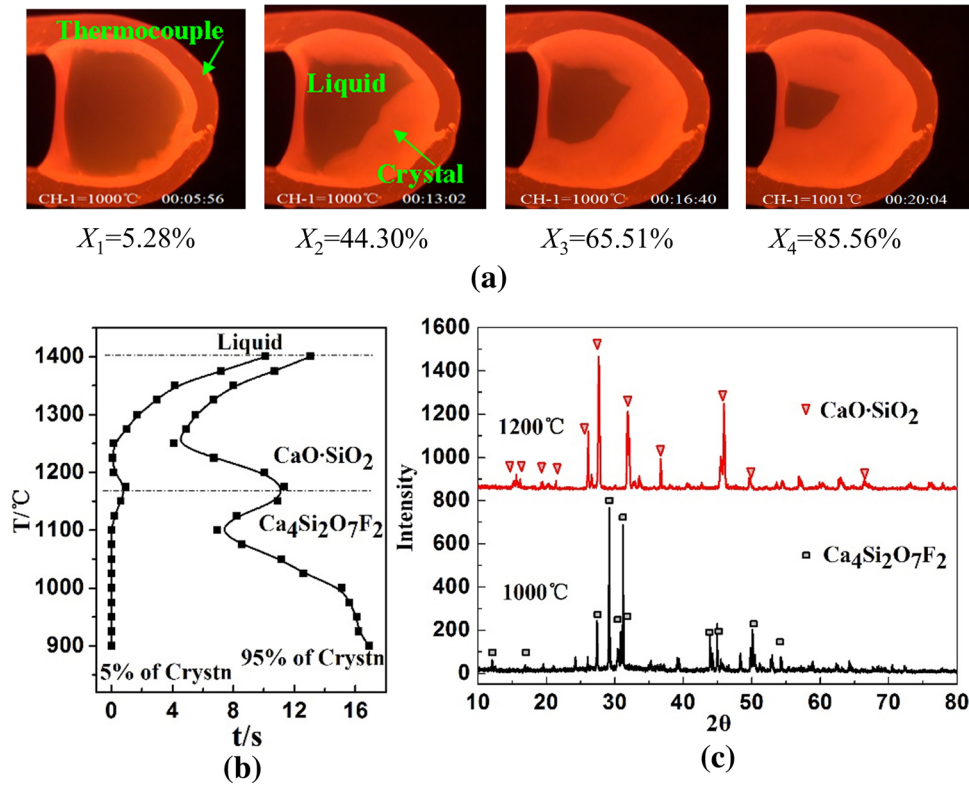


Fig. 3. Investigation of isothermal crystallization process of mold flux using the SHTT:<sup>65</sup> (a) snapshots, (b) TTT diagram, and (c) precipitate crystalline phase.

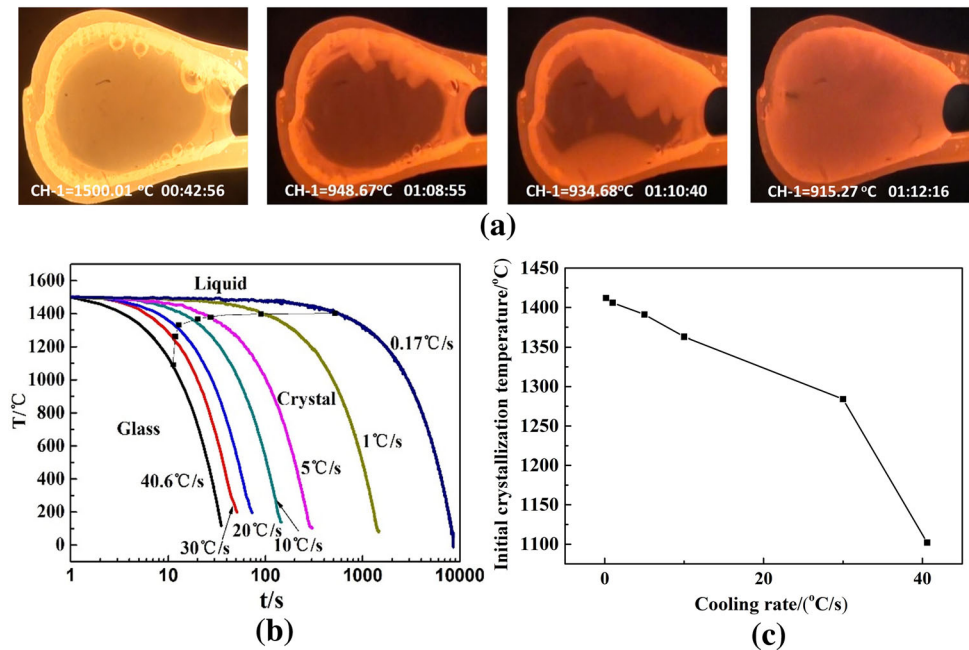


Fig. 4. Investigation of nonisothermal crystallization process of mold flux using the SHTT:<sup>65,76</sup> (a) snapshots, (b) CCT diagram, and (c) initial crystallization temperature at different cooling rates.

traditional methods and techniques cannot create such temperature fields, but the double hot-thermocouple technique (DHTT) has been successfully developed to simulate such temperature

distributions, by separately controlling the temperatures of two thermocouples, with one being high and the other low. The key point when utilizing the DHTT to simulate such a temperature field is to

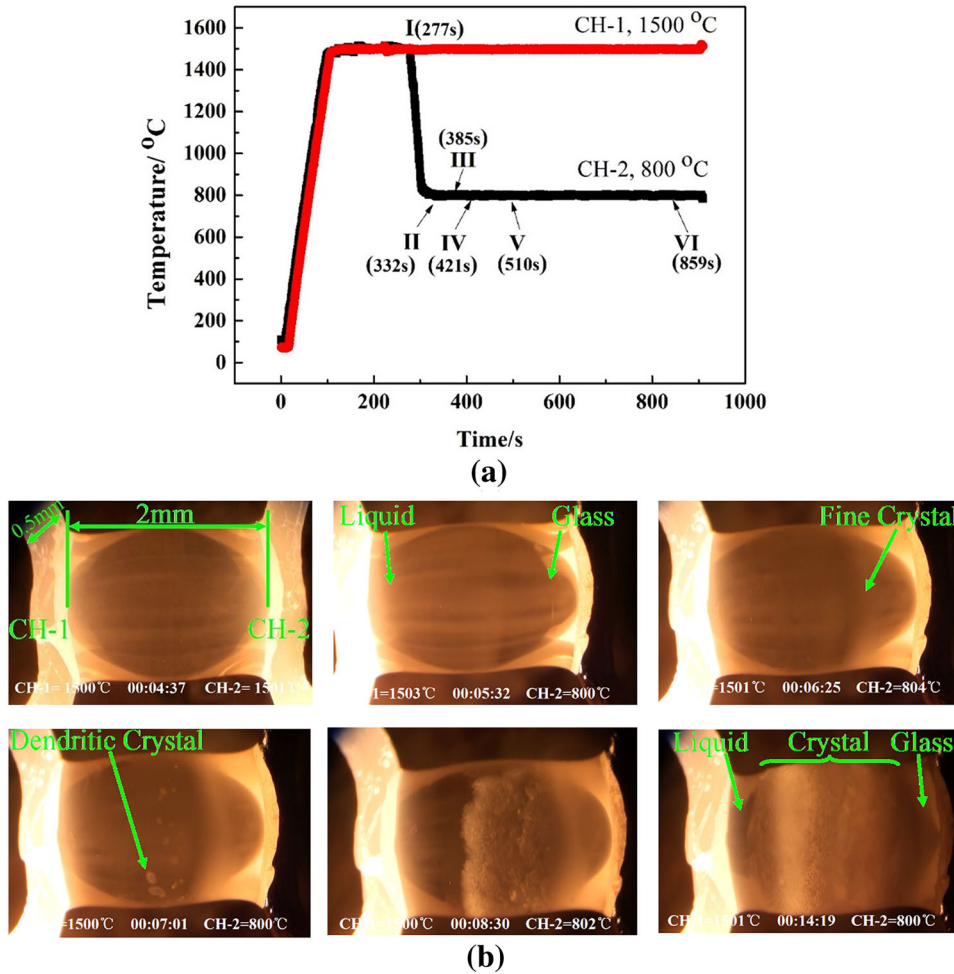


Fig. 5. Phase evolution of mold flux under simulated temperature field using the DHTT.<sup>80,81</sup> (a) temperature controlling process and (b) typical stages of phase evolution.

determine the exact temperatures to which the two thermocouples should be set and the distance them. Figure 5 shows the temperature controlling process and snapshots of typical stages of phase evolution under the simulated temperature field as measured using the DHTT.<sup>80,81</sup>

In Fig. 5, the hot thermocouple (CH-1) is used to simulate the solidified shell surface and is set at 1773 K (1500°C) according to previous reports.<sup>82,83</sup> The cold thermocouple (CH-2) is used to simulate the solid slag film surface close to the mold wall; the temperature of the cold thermocouple,  $T_{INT}$ , can be estimated using Eq. 1,<sup>73,84</sup>

$$T_{INT} = T_{HM} - q_T \times R_{INT} \quad (1)$$

where  $T_{HM}$  is the temperature of the hot-side mold wall,  $q_T$  is the heat flux across the mold flux, and  $R_{INT}$  is the interfacial thermal resistance. The values for  $q_T$ ,  $T_{HM}$ , and  $R_{INT}$  are obtained from previous studies.<sup>44,80,81,85–89</sup> Consequently, the temperature of CH-2 ( $T_{INT}$ ) is determined to be 1073 K (800°C). Besides, the distance between the two thermocouples is set as 2 mm.<sup>72,83</sup>

The results shown in Fig. 5 can be used to observe and study the phase evolution in situ during the period when the liquid mold flux infiltrates into the shell–mold gap in the vicinity of the meniscus. Based on this approach, the evolution and distribution of liquid, crystalline, and glassy layers of mold flux in the gap can be obtained intuitively by controlling the temperatures of the two thermocouples properly.

## WETTING BEHAVIOR

Continuous casting is a complex process involving multiple coexisting phases and transformations, including liquids (molten steel and slag), solids (mold wall, nozzle, shell, mold flux powders, inclusions, etc.), and gases (argon, CO/CO<sub>2</sub>, O<sub>2</sub>, N<sub>2</sub>, H<sub>2</sub>, etc.). These complex phases undergo complex chemical and physical interactions in the mold under transient and high-temperature conditions. Therefore, the surface and interfacial properties of the mold flux have a significant impact on the continuous casting process, affecting surface waves on the top of the mold,<sup>90,91</sup> entrapment of inclusions,<sup>92</sup> slag

emulsion,<sup>93,94</sup> and bubbles,<sup>95</sup> as well as nozzle clogging in the mold,<sup>96</sup> etc. X-ray photography and the sessile drop method are the two major methods applied to investigate the surface and interfacial properties of mold flux. Among these, x-ray photography can be used to observe and study the interfacial properties between two liquid phases by transmission photography using x-rays, whereas the sessile drop method is suited to analyze the interfacial properties between a liquid and solid by measuring the contact angle.

The SHTT can also be utilized to study the surface and interfacial properties of mold flux by observing the wetting behavior of molten mold flux on platinum–rhodium wire (B-type thermocouple) and measuring the contact angle. Figure 6 shows a typical result for a mold flux droplet on the surface of a B-type thermocouple, showing a contact angle of 39° in this case. Therefore, the influence of compo-

sition, temperature, and atmosphere on the surface and interfacial properties of mold flux can also be investigated based on this method.

### HEAT TRANSFER

The heat transfer from the molten steel pool to the mold wall directly determines the initial solidification of the molten steel, since the fundamental function of the continuous casting process is to release its latent and super heat. Improper heat transfer performance of mold flux can result in additional thermal stress on the solidified shell, introducing slab surface defects.<sup>97</sup> The infrared emitter technique (IET) and copper finger heat flux simulator utilize embedded thermocouples to measure the response temperatures inside the water-cooled copper mold or the inlet/outlet cooling water temperatures to calculate the heat flux across the mold flux film. Meanwhile, the FTIR spectrometry method characterizes the heat transfer ability by measuring the reflectivity (Ra) and transmissivity (Ta) of samples. The principle of using the DHTT to study the heat transfer behavior of mold flux is similar to the laser-pulse technique. During the test process, the slag is mounted between the two thermocouples and kept at a certain temperature, then a temperature pulse, e.g., 200 K, is applied from one thermocouple, while the response temperature is recorded by the other. This response can then be used to evaluate the heat transfer ability of the tested slag sample.

Figure 7 shows an example of two mold flux samples being evaluated by the DHTT.<sup>98</sup> It can be seen from Fig. 7 that the response temperatures for Flux2 are higher than those for Flux1, indicating

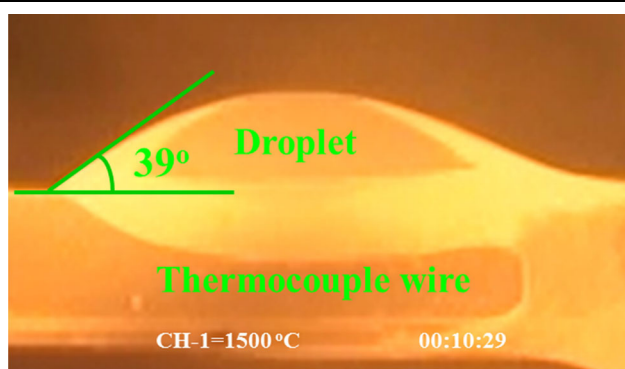


Fig. 6. Wetting behavior of mold flux droplet on platinum–rhodium wire.

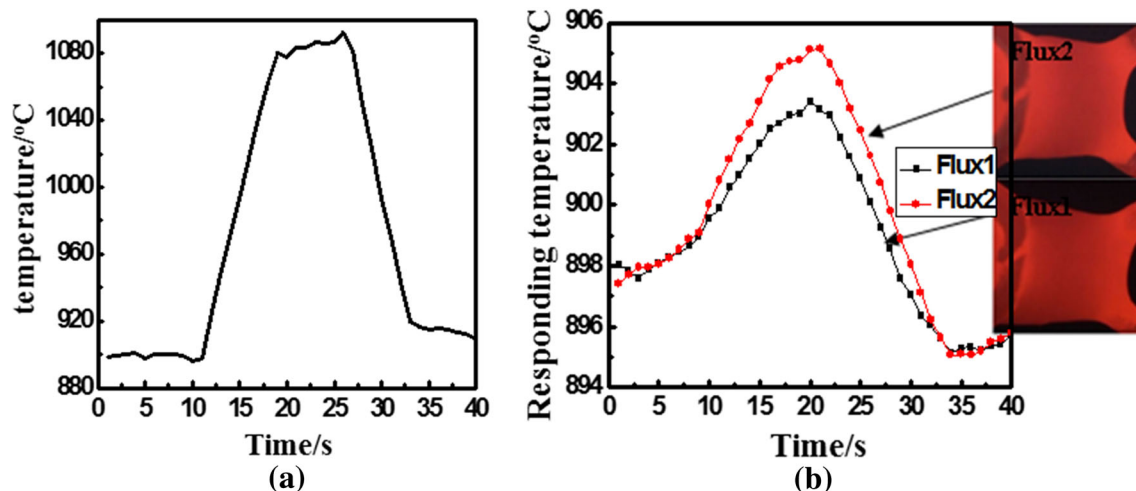


Fig. 7. Heat transfer ability of mold flux evaluated using the DHTT:<sup>98</sup> (a) temperature pulse and (b) response temperatures when the temperature pulse is imposed.

that the Flux2 film exhibits better thermal transfer ability, leading to the higher response temperature than Flux1.

## CONCLUSIONS

The single/double hot-thermocouple techniques (S/DHTT) have become routine methods for investigating the high-temperature properties of mold flux. In this paper, extensive research works related to the S/DHTT have been summarized; the following main conclusions can be drawn:

1. The initial and complete melting temperatures of mold flux can be obtained using the SHTT by combing the temperature deviation between the preset heating rate and that measured in real time with in situ observations of the variation of the appearance of the real sample.
2. The SHTT can achieve high heating and cooling rates, which is necessary to effectively simulate the real scenario in the mold and facilitates investigation of isothermal and nonisothermal crystallization processes of mold flux. Isothermal and nonisothermal crystallization transformation can be well studied by constructing TTT and CCT diagrams, as well as further kinetic analysis.
3. The huge temperature gradient in the gap between the hot solidified shell and water-cooled mold wall can be simulated using the DHTT, by separately controlling the temperatures of two thermocouples, with one being high and one low. This approach enables the evolution and distribution of liquid, crystalline, and glassy layers of mold flux film in the gap to be investigated intuitively.
4. The SHTT can also be utilized to study the surface and interfacial properties of mold flux by observing the wetting behavior of molten mold flux on platinum–rhodium wire (B-type thermocouple) and measuring the contact angle. Moreover, the heat transfer ability of mold flux can be evaluated using the DHTT by applying a temperature pulse from one thermocouple and recording the response temperature using the other.

## ACKNOWLEDGEMENTS

Financial support from the National Science Foundation of China (51504294, U17060202) and the Opening Foundation of the Ministry of Education Key Laboratory of Metallurgical Emission Reduction & Resources Recycling (Anhui University of Technology) is greatly acknowledged.

## REFERENCES

1. E. Basson, *World Steel in Figures 2017* (Brussels: World Steel Association, 2017), pp. 1–26.
2. E. Takeuchi and J.K. Brimacombe, *Metall. Mater. Trans. B* 15, 493 (1984).
3. J. Sengupta, H.J. Shin, B.G. Thomas, and S.H. Kim, *Acta Mater.* 54, 1165 (2006).
4. L. Zhou, W. Wang, C. Xu, and C. Zhang, *Metall. Mater. Trans. B* 48, 1 (2017).
5. P.E. Ramirez-Lopez, K.C. Mills, P.D. Lee, and B. Santillana, *Metall. Mater. Trans. B* 43, 109 (2012).
6. S. Harada, S. Tanaka, H. Misumi, S. Mizoguchi, and H. Horiguchi, *ISIJ Int.* 30, 310 (1990).
7. X. Long, S. He, and Q. Wang, *Metall. Mater. Trans. B* 48, 1652 (2017).
8. J. Konishi, M. Militzer, J.K. Brimacombe, and I.V. Samarasera, *Metall. Mater. Trans. B* 33, 413 (2002).
9. B.G. Thomas, Q. Yuan, S. Mahmood, R. Liu, and R. Chaudhary, *Metall. Mater. Trans. B* 45, 22 (2014).
10. L. Zhang and B.G. Thomas, *Metall. Mater. Trans. B* 37, 733 (2006).
11. A. Kumar, S.K. Choudhary, and S.K. Ajmani, *ISIJ Int.* 52, 2305 (2012).
12. X. Deng, L. Li, X. Wang, Y.G. Ji, C. Ji, and G. Zhu, *Int. J. Miner. Met. Mater.* 21, 531 (2014).
13. J.W. Elmer, S.M. Allen, and T.W. Eagar, *Metall. Mater. Trans. A* 20, 2117 (1989).
14. L. Zhou and W. Wang, *JOM* 66, 1595 (2014).
15. C.A. Muojekwu, I.V. Samarasekera, and J.K. Brimacombe, *Metall. Mater. Trans. B* 26, 361 (1995).
16. W. Wang, C. Zhu, and L. Zhou, *Steel Res. Int.* (2017). <https://doi.org/10.1002/srin.201600488>.
17. S. Sridhar, K.C. Mills, O.D.C. Afrange, H.P. Lörz, and R. Carli, *Ironmak. Steelmak.* 27, 238 (2000).
18. B. Li and F. Tsukihashi, *Trans. Iron Steel Inst. Jpn.* 45, 30 (2006).
19. A. Sanz, *Surf. Coat. Technol.* 146, 55 (2001).
20. E. Wei, Y. Yang, C. Feng, I. Somerville, and A. Mclean, *J. Iron. Steel Res. Int.* 13, 22 (2006).
21. G. Wen, S. Sridhar, P. Tang, X. Qi, and Y. Liu, *ISIJ Int.* 47, 1117 (2007).
22. J. Qi, C. Liu, D. Yang, C. Zhang, and M. Jiang, *Steel Res. Int.* 87, 890 (2016).
23. L. Zhou, H. Li, and W. Wang, *Steel Res. Int.* (2017). <https://doi.org/10.1002/srin.201600459>.
24. S. Esfahani, K. Danaei, D. Budurea, and M. Barati, *Meas. Sci. Technol.* 27, 1 (2016).
25. L. Zhou, W. Wang, J. Wei, and K. Zhou, *ISIJ Int.* 55, 821 (2015).
26. H. Nakada and K. Nagata, *ISIJ Int.* 46, 441 (2006).
27. M. Hanao, M. Kawamoto, and T. Watanabe, *ISIJ Int.* 44, 827 (2007).
28. R. Hill, N. Costa, and R. Law, *J. Non-Cryst. Solids* 351, 69 (2005).
29. X. Jiang, M. Engelhard, K. Ataka, and J. Heberle, *Metall. Mater. Trans. B* 41, 805 (2010).
30. W. Wang, X. Yan, L. Zhou, S. Xie, and D. Huang, *Metall. Mater. Trans. B* 47, 963 (2016).
31. J. Yang, Y. Cui, L. Wang, Y. Sasaki, J. Zhang, O. Ostrovski, and Y. Kashiwaya, *Steel Res. Int.* 86, 636 (2015).
32. L. Zhou, W. Wang, and K. Zhou, *Metall. Mater. Trans. E* 2, 99 (2015).
33. G. Wen, H. Liu, and P. Tang, *J. Iron. Steel Res. Int.* 15, 32 (2008).
34. W. Yan, W. Chen, Y. Yang, C. Lippold, and A. Mclean, *ISIJ Int.* 55, 1000 (2015).
35. J.Y. Park, J.W. Ryu, and I. Sohn, *Metall. Mater. Trans. B* 45, 1186 (2014).
36. Z. Zhang, J. Li, and P. Liu, *J. Iron. Steel Res. Int.* 18, 31 (2011).
37. A.B. Fox, M.E. Valdez, J. Gisby, R.C. Atwood, P.D. Lee, and S. Sridhar, *ISIJ Int.* 44, 836–845 (2004).
38. L. Zhou, W. Wang, and K. Zhou, *Metals* 6, 139 (2016).
39. J. Yang, J. Zhang, Y. Sasaki, O. Ostrovski, C. Zhang, D. Cai, and Y. Kashiwaya, *Metall. Mater. Trans. B* 47, 2447 (2016).
40. D. Yoon, J. Cho, and S. Kim, *Metall. Mater. Trans. B* 48, 1 (2017).

41. L. Zhou, W. Wang, J. Wei, and M. Jin, *ISIJ Int.* 53, 665 (2013).
42. H. Ryu, Z. Zhang, J. Cho, G. Wen, and S. Sridhar, *ISIJ Int.* 50, 1142 (2010).
43. X. Qi, G. Wen, and P. Tang, *J. Non-Cryst. Solids* 354, 5444 (2008).
44. J. Cho, H. Shibata, T. Emi, and M. Suzuki, *ISIJ Int.* 38, 268 (1998).
45. J. Diao, B. Xie, J. Xiao, and C. Ji, *ISIJ Int.* 49, 1710 (2009).
46. J. Diao, B. Xie, N. Wang, S. He, Y. Li, and F. Qi, *ISIJ Int.* 47, 1294 (2007).
47. M. Susa, A. Kushimoto, R. Endo, and Y. Kobayashi, *ISIJ Int.* 51, 1587 (2011).
48. Y. Chung and A. Cramb, *Metall. Mater. Trans. B* 31, 957 (2000).
49. V. Chevrier and A. Cramb, *Metall. Mater. Trans. B* 31, 537 (2000).
50. L. Zhou, J. Li, W. Wang, and I. Sohn, *Metall. Mater. Trans. B* 48, 1943 (2017).
51. W. Wang, J. Li, L. Zhou, and J. Yang, *Met. Mater. Int.* 22, 700 (2016).
52. E. Jung, W. Kim, I. Sohn, and D. Min, *J. Mater. Sci.* 45, 2023 (2010).
53. S. Shin, J. Cho, and S. Kim, *J. Am. Ceram. Soc.* 97, 3263 (2015).
54. L. Zhou and W. Wang, *Metall. Mater. Trans. B* 48, 220 (2017).
55. L. Zhou and W. Wang, *Metall. Mater. Trans. B* 47, 1548 (2016).
56. F. Ordway, *J. Res. Natl. Bur. Stand.* 48, 152 (1952).
57. J. Welch, *J. Sci. Instrum.* 48, 458 (1954).
58. W. Gutt, *Nature* 190, 339 (1961).
59. P. Hart and E. Steward, *J. Inorg. Nucl. Chem.* 24, 633 (1962).
60. D. Burnett, D. Clinton, and R. Miller, *J. Mater. Sci.* 3, 47 (1968).
61. A. Maries and P. Rogers, *J. Mater. Sci.* 13, 2119 (1978).
62. N. Odling, *Mineral. Mag.* 59, 267 (1995).
63. Y. Kashiwaya, C. Cicutti, and A. Cramb, *Trans. Iron Steel Inst. Jpn.* 38, 357 (1998).
64. Y. Kashiwaya, C. Cicutti, A. Cramb, and K. Ishii, *ISIJ Int.* 38, 348 (1998).
65. L. Zhou, W. Wang, F. Ma, J. Li, J. Wei, H. Matsuura, and F. Tsukihashi, *Metall. Mater. Trans. B* 43, 354 (2012).
66. N. Kölbl and H. Harmuth, *J. Mater. Sci.* 46, 6248 (2011).
67. S. Sridhar, K.C. Mills, and S.T. Mallaband, *Ironmak. Steelmak.* 29, 194 (2002).
68. B. Ozturk, *Metall. Trans. B* 23, 523 (1992).
69. K.C. Mills and A.B. Fox, *ISIJ Int.* 43, 1479 (2003).
70. C. Moynihan, A. Easteal, J. Wilder, and J. Tucker, *J. Phys. Chem.* 78, 2673 (1974).
71. L. Zhou, W. Wang, B. Lu, and G. Wen, *Met. Mater. Int.* 21, 126 (2015).
72. K. Mills, A. Fox, Z. Li, and R. Thackray, *Ironmak. Steelmak.* 32, 26 (2005).
73. W. Wang, Ph.D. dissertation, Carnegie Mellon University, (2007).
74. J. Li, X. Wang, and Z. Zhang, *ISIJ Int.* 51, 1396 (2011).
75. Z. Wang, Q. Shu, and K. Chou, *Metall. Mater. Trans. B* 44, 606 (2013).
76. L. Zhou, H. Li, W. Wang, Z. Wu, J. Yu, and S. Xie, *Metall. Mater. Trans. B* 48, 2949 (2017).
77. Y. Sun, H. Shen, H. Wang, X. Wang, and Z. Zhang, *Energy* 76, 761 (2014).
78. R. Carli and C. Righi, in *VII International Conference on Molten Slags Fluxes and Salts* (South African: JSAMAP, 2004), p. 821.
79. M. Seo, C. Shi, H. Wang, J. Cho, and S. Kim, *J. Non-Cryst. Solids* 412, 58 (2015).
80. L. Zhou, W. Wang, D. Huang, J. Wei, and J. Li, *Metall. Mater. Trans. B* 43, 925 (2012).
81. L. Zhou, W. Wang, R. Liu, and B.G. Thomas, *Metall. Mater. Trans. B* 44, 1264 (2013).
82. A.W. Cramb, Quantifying the thermal behavior of slags (Report: American Iron and Steel Institute, Technology Roadmap Program, Pittsburgh, PA, USA, 2003).
83. Y. Meng and B.G. Thomas, *Metall. Mater. Trans. B* 34, 707 (2003).
84. B. Coates and S.A. Argyropoulos, *Metall. Mater. Trans. B* 38, 243 (2007).
85. P.E. Ramirez-Lopez, P.D. Lee, and K.C. Mills, *ISIJ Int.* 50, 1797 (2010).
86. P.E. Ramirez-Lopez, P.D. Lee, and K.C. Mills, *ISIJ Int.* 50, 425 (2010).
87. Y. Meng and B.G. Thoma, *Metall. Mater. Trans. B* 34, 685 (2003).
88. D.T. Stone and B.G. Thomas, *Can. Metall. Q.* 38, 363 (1999).
89. J. Cho, H. Shibata, T. Emi, and M. Suzuki, *ISIJ Int.* 38, 440 (1998).
90. J. Anagnostopoulos and G. Bergeles, *Metall. Mater. Trans. B* 30, 1095 (1999).
91. K.C. Mills, E.D. Hondros, and Z. Li, *J. Mater. Sci.* 40, 2403 (2005).
92. P. Rocabois, J. Lehmann, C. Gatellier, and J.P. Teres, *Ironmak. Steelmak.* 30, 95 (2003).
93. R. Hagemann, H.P. Heller, S. Lachmann, S. Seetharaman, and P.R. Scheller, *Ironmak. Steelmak.* 39, 508 (2012).
94. L.C. Hibbeler and B.G. Thomas, *Iron Steel Technol.* 10, 121 (2013).
95. Y. Miki and S. Takeuchi, *ISIJ Int.* 43, 1548 (2003).
96. C.G. Aneziris, E.M. Pfaff, and H.R. Maier, *J. Eur. Ceram. Soc.* 20, 159 (2000).
97. J. Kelly, K. Michalek, B. Thomas, and J. Dantzig, *Metall. Mater. Trans. A* 19, 2589 (1988).
98. W. Wang, K. Gu, L. Zhou, F. Ma, I. Sohn, D. Min, H. Matsuura, and F. Tsukihashi, *ISIJ Int.* 51, 1838 (2011).